Case 2 waters: the challenges of spectral optimization for chlorophyll retrieval

Christopher P Kuchinke, Howard R Gordon, Kenneth J Voss
Atmospheric and Ocean Optics Group
Department, of Physics, University of Miami, FL 33124

Background

The spectral optimization algorithm (SOA) was originally developed for processing SeaWiFS and MODIS data in Case 1 waters (Chomko et al. 2003).

Atmospheric particles are characterized according to their diameter, concentration (for discrete size intervals) and Junge size distribution parameter *v*. The optical properties of the aerosol are then computed from Mie theory using the given size distributions and the complex index of refraction $m = m_r - m_i$.

The Garver and Siegel (1997) bio-optical model retrieves three parameters: (1) the absorption coefficient of colored detrital matter at 443-nm ($a_{cdm}(443)$); (2) the chlorophyll *a* concentration *C*, and (3) the backscattering coefficient of particulate matter at 443-nm ($b_{bp}(443)$).

SOA couples both atmospheric aerosol and bio-optical models to simultaneously retrieve both atmospheric (m_i, m_r) and ocean color parameters (*C*, a_{cdm}, b_{bp}).

The model has been recently configured to operate in Case 2 waters. First we assume Case 1 waters and operate the algorithm. The retrieved values of *C*, $a_{cdm}(443)$ and $b_{bp}(443)$ are then used to provide an estimate of r_w in the NIR, and the retrieved values of *v*, optical depth t_a, m_r and m_i are used to estimate diffuse transmittances t_v and t_s in the NIR. $t_s t_v r_w$(NIR) is then subtracted from the total reflectance in the NIR (less Rayleigh scattering $r_r(\lambda)$) and the process repeated until $r_w(865)$ is stable.

Case 1 status

The optimization attempts to find water and atmospheric parameters that provide the best fit between modeled reflectance $r_A(\lambda)+t_s t_v r_w(\lambda)$ and measured reflectance $r_t(\lambda)-r_r(\lambda)$ in a least squares sense $f_{lsq}(\lambda)$. We then define the sum across all channels as f_{lsq}. The non-linear optimization procedure utilized by SOA was configured to provide an accuracy that is dependent on the machine precision of the code. Generally speaking, this produced a better than one percent agreement between $r_t(\lambda)-r_r(\lambda)$ and $r_A(\lambda)+t_s t_v r_w(\lambda)$. Generally speaking, SOA performs well in absorbing atmospheres and situations where $a_{cdm}(443) < 0.05$ m^{-1} (Case 1 waters). Results here have been validated with both the Gordon and Wang (1994) model and LIDAR measurements (Chomko et al. 2003).

Case 2 status

The algorithm will often fail at the one percent precision level in Case 2 waters. We define failure here as the situation where any of the given parameters *C*, $a_{cdm}(443)$, b_{bp}, m_r or m_i are driven to an upper or lower boundary in the algorithm. Generally speaking, this precision is beyond the accuracy of both the constraining models AND the satellite measurements. For example, if the atmosphere is devoid of absorbing aerosol the satellite sensor receives a reduced signal at the NIR wavelengths. This exacerbates any error in the estimation of $r_A(\lambda)$ at the blue wavelengths. If the water column is also relatively 'dark' due to high a_{cdm}, then an f_{lsq} of less than 5% at visible wavelengths (SeaWiFS channels 1 to 6) is unrealistic and likely to result in erroneous results in order to achieve this precision.

Current model improvement

Of the 'free' parameters used here, SOA is most sensitive to b_{bp} and least sensitive to m_r, m_i and a_{cdm} in respective order. For $f_{lsq} < 5\%$, SOA will reduce b_{bp} BEFORE destabilizing m_i or a_{cdm}. Stability is defined as the 'inertia' of a free parameter as the optimization proceeds or 'iterates'. Preliminary scene analysis suggests that stable values of m_i and a_{cdm} are reached during the optimization iterations and BEFORE a high precision f_{lsq} is reached. The subsequent reduction in 'candidate' b_{bp} is viewed as an artifact of the unrealistic f_{lsq} and often leads to *C* failure for the situations discussed earlier.

We address this situation through development of a scheme designed to 'stop' the optimization earlier. At each pixel, we select stability of 'insensitive' free parameters as the criteria for this purpose. Recent tests reveal that this approach is more robust for a particular scene as opposed to setting the same lower threshold for f_{lsq} across the all pixels. In this poster, we illustrate the results of using criteria $g''(m_i)$ to stop the optimization, a second order derivative where

$$g(m_i) = dr/dmi = \hat{A}_{\lambda} [\, (dflsq(\lambda)/dr(\lambda) \;/\; (dr/dm_i)\,],$$

$$dr/dm_i = dr_{Ac}(\lambda)/dm_i + r_w * [dt_s(\lambda)/dm_i * t_v(\lambda) + t_s(\lambda) * dt_v(\lambda)/dm_i]$$

and $r_{Ac}(\lambda)$ is the 'candidate' aerosol reflectance for a particular wavelength.

Figures 1a to c are *C* (mg m^{-3}) images processed using SeaWiFS data for day 93-2000 off Santa Monica Bay and surrounding waters. Figure 1a uses the Gordon and Wang (1994) atmospheric correction (STD) and OC4 visible band ratios for the ocean (O'Reilly et al. 1998). Figure 1b utilizes SOA and stability in $g''(m_i)$ as the 'stop' criteria for the optimization at each pixel ($1\% < f_{lsq} < 5\%$). Results here indicate some success as indicated by the similar spatial variability across the image. Areas of 'noise' still remain and is the focus of current analysis. Figure 1c shows SOA in high machine precision mode ($f_{lsq} < 0.5\%$) and indicates pixel failure for most of the displayed coastline. Figures 2a and b are the same as Figures 1b and c but for day 303-1997. SOA results here suggest that stopping the optimization earlier is having some success. Figure 2a contains no failed pixels and greater structural detail in *C* than Figure 2b.

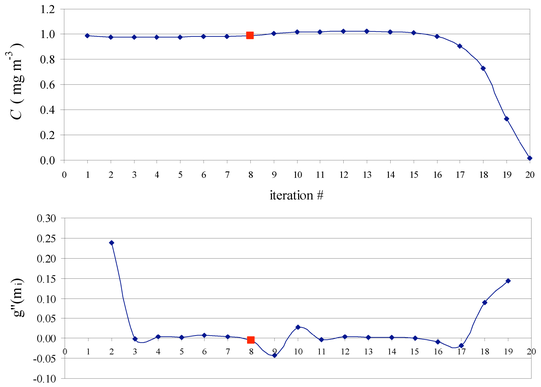

Figure 3. Failed pixel example. SOA iteration number versus *C* and $g''(m_i)$. Optimization stopped at red marker.

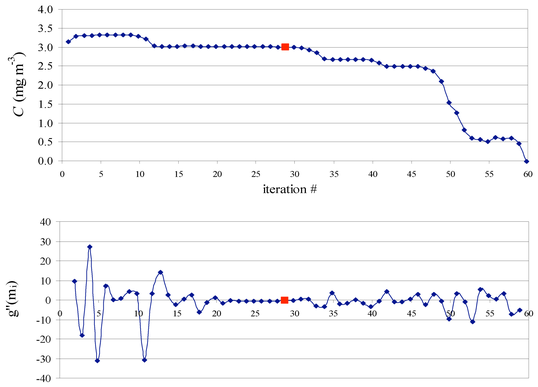

Figure 4. Same as Figure 3 but for a different pixel.

Figures 3 and 4 depict the optimization (search) status of *C* and $g''(m_i)$ as a function of iteration number for two different pixels. In both examples *C* fails if the iterations continue until flsq and the machine precision converge (the final iteration in the figures). Note that stability in $g''(m_i)$ is correlated with changes in *C* and defined plateaus can be seen in both *C* graphs.

Current code starts with a small $g''(m_i)$ filter and looks for the first group of consecutive iterations that lie in the selected $g''(m_i)$ filter zone. If none are found then the $g''(m_i)$ filter is increased and the search repeated. This procedure is independent from pixel to pixel and ensures that the most stable $g''(m_i)$ zone at each pixel is always found. The red markers in Figures 3 and 4 indicate where SOA is 'stopped' given the present algorithm. Figure 3 shows that the algorithm could be altered to selected the second $g''(m_i)$ zone and produce a similar value of *C*. However in the $g''(m_i)$ transition (iterations 8 to 10) candidates m_i and $a_{cdm}(443)$ would change to different plateaus (one increasing, the other decreasing). This illustrates one of the challenges one is faced with when using optimization techniques for high quality analysis of this nature.

Note that this procedure nearly always results in low f_{lsq} (< 5%) for all pixels at the 'stopped' iteration . The only exception is for pixels characterized by a very 'clear' atmosphere (no aerosol absorption) and very high a_{cdm}. Under these conditions the satellite signal becomes very low and final f_{lsq} is of the order of 20%. This results in an incomplete decoupling of r_A and r_w producing too low and high a_{cdm} and m_i respectively. Although not implemented in the images presented here, we alleviate this problem by reducing the weighting of $f_{lsq}(412)$ in SOA. This allows the fit between $r_t(412)$-$r_r(412)$ and $r_A(412)+t_s t_v r_w(412)$ to vary by over 50% and composite f_{lsq} (for all visible bands) to again conform to a 5% tolerance. ie. $f_{lsq}(\lambda)$ at bands 2 to 6 are of the order of 1 to 3%.

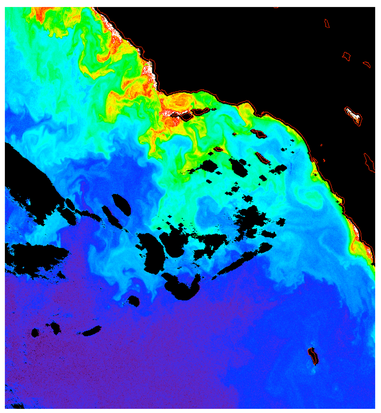

Figure 1a. STD(OC4) retrieved *C* (mg m^{-3}) for SeaWiFS day 93-2000. Santa Monica Bay and surrounding waters.

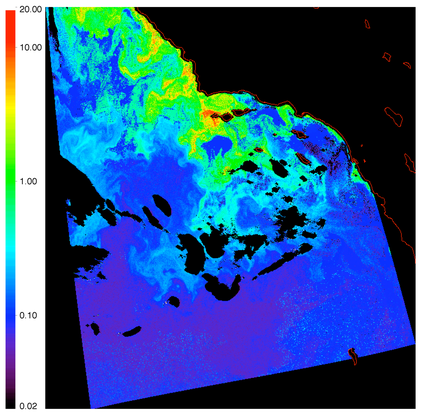

Figure 1b. SOA retrieved *C* (mg m^{-3}) for SeaWiFS day 93-2000. Santa Monica Bay and surrounding waters. $g''(m_i)$ optimization 'stop' criteria at each pixel.

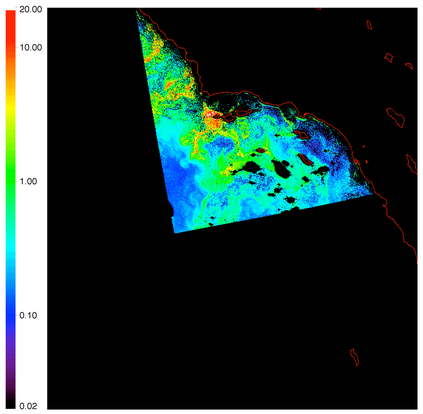

Figure 1c. Same as Figure 1b. f_{lsq} at each pixel determined by the machine precision.

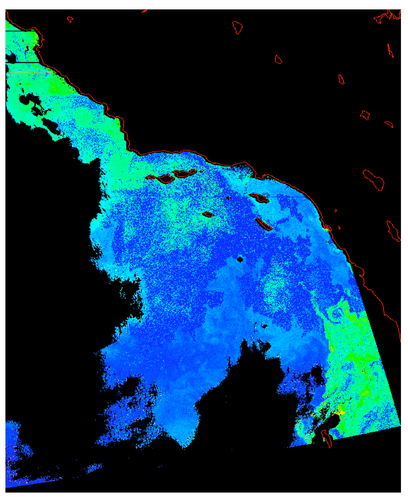

Figure 2a. SOA retrieved *C* (mg m^{-3}) for SeaWiFS day 303-1997. Santa Monica Bay and surrounding waters. $g''(m_i)$ optimization 'stop' criteria at each pixel.

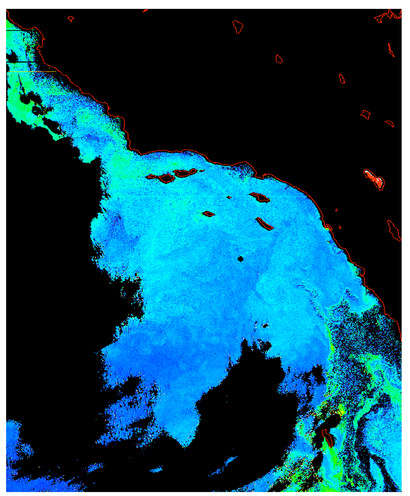

Figure 2b. Same as Figure 2a. f_{lsq} at each pixel determined by the machine precision.

Concluding Remarks

The SOA scheme has the potential to work in atmospheres characterized by absorbing aerosols, an improvement to the standard algorithms currently in use. Current focus is on refinement of the analysis presented here with results expected shortly.

Acknowledgements

This work was prepared by University of Miami under award #NA17RJ1226 from NOAA/NESDIS, U.S. Department of Commerce.

References

Chomko, R.M., H.R. Gordon, S. Maritorena, and D.A. Siegel (2003): Simultaneous retrieval of oceanic and atmospheric parameters for ocean color imagery by spectral optimization: a validation, Remote Sensing of Environment, 84, 208-220.

Garver, S., and D. Siegel (1997): Inherent optical property inversion of ocean color spectra and its biogeochemical interpretation: 1 time series from the Sargasso Sea, Jour. Geophys. Res., 102C, 18607-18625.

Gordon, H.R., and M. Wang (1994): Retrieval of water-leaving radiance and aerosol optical thickness over the oceans with SeaWiFS: a preliminary algorithm, Applied Optics, 33, 443-452.

O'Reilly, J.E., S. Maritorena, B.G. Mitchell, D.A. Siegel, K.L. Carder, S.A. Garver, M. Kahru, and C. McClain (1998): Ocean color chlorophyll algorithms for SeaWiFS, Jour. Geophys. Res., 103C, 24937-24953.